Computational performance of the $MMOC$ in the inverse design of the Doswell frontogenesis equation

Alexandre Francisco[a,*], Umberto Biccari[b], Enrique Zuazua[b]

[a] *Department of Mechanical Engineering, Universidade Federal Fluminense, 27255-125, Volta Redonda, RJ, Brazil*
[b] *Chair of Computational Mathematics, University of Deusto, 48007, Bilbao, Basque Country, Spain*

Abstract

Inverse design of transport equations can be addressed by using a gradient-adjoint methodology. In this methodology numerical schemes used for the adjoint resolution determine the direction of descent in its iterative algorithm, and consequently the CPU time consumed by the inverse design. As the CPU time constitutes a known bottleneck, it is important to employ light and quick schemes to the adjoint problem. In this regard, we proposed to use the Modified Method of Characteristics ($MMOC$). Despite not preserving identity conservation, the $MMOC$ is computationally competitive. In this work we investigated the advantage of using the $MMOC$ in comparison with the Lax-Friedrichs and Lax-Wendroff schemes for the inverse design problem. By testing the Doswell frontogenesis equation, we observed that the $MMOC$ can provide more efficient and accurate computation under some simulation conditions.

Keywords: Characteristics-based method, inverse design, Doswell frontogenesis.
2020 MSC: 00-01, 99-00

1. Introduction

The problem of inverse design of transport equations can be addressed by using gradient-adjoint methodologies. Recently, Morales-Hernandez and Zuazua

*Corresponding author
Email address: afrancisco@id.uff.br (Alexandre Francisco)

[1] investigated the convenience of using low-order numerical schemes for the adjoint resolution in the gradient-adjoint methodology. They focused on linear scalar transport equations with heterogeneous time-independent flux functions.

Morales-Hernandez and Zuazua analysed the numerical resolution of the adjoint problem by means of first-order and second-order numerical schemes. They concluded that first-order schemes are the best choices when dealing with smooth functions since second-order schemes introduce high frequencies and spurious oscillations in the solution. In addition, first-order schemes require shorter CPU times than second-order ones.

The numerical scheme used for the adjoint resolution determines the descent direction in the gradient-adjoint method [1], and consequently it influences the CPU time consumed by the iterative algorithm. As the CPU time constitutes a known bottleneck, we proposed a characteristic-based method, the called Modified Method of Characteristics ($MMOC$) [2], for efficient adjoint resolutions. The $MMOC$ is based on the characteristic curves and so is very computationally competitive for linear transport equations. Zhang et al. [3] has demonstrated that the $MMOC$ is feasible and reliable in forward and inverse simulations of underwater explosion, for example.

The Doswell frontogenesis problem is a linear equation in which a non-uniform and time-dependent flow gives rise a challenging solution to be simulated. It allows to assess the performance of inverse design simulations in the treatment of moving vortex-type surfaces in two dimensions. The Doswell frontogenesis equation can be used to describe the presence of horizontal temperature gradients and fronts in the context of meteorological dynamics.

We performed numerical simulations in order to investigate the $MMOC$ for solving the Doswell frontogenesis problem. In this work the adjoint problem is also a linear equation, worthing the use of the characteristic-based method. For comparisons with the $MMOC$, we used the first-order Lax-Friedrichs (LF) and the second-order Lax-Wendroff (LW) schemes. The $MMOC$ provided shorter CPU time and smaller error than the LF and LW schemes, under some simulation conditions. Thus, the $MMOC$ can be an efficient and accurate

scheme for addressing the inverse design problem.

This work is presented as follows: this introduction is followed by a summarized development of the gradient-adjoint methodology for the problem of inverse design of transport equations. Next, the $MMOC$ is introduced for solving linear transport equations. Afterwards, the efficiency and accuracy of the $MMOC$ is evaluated in comparison with the LF and LW for the Doswell frontogenesis equation. Finally, the conclusions about the performance of the $MMOC$ are presented.

2. The gradient-adjoint methodology

Consider the following transport problem with a given time-independent vector field $\mathbf{v} = \mathbf{v}(\mathbf{x})$:

$$\frac{\partial u}{\partial t} + \nabla \cdot (\mathbf{v}u) = 0, \quad u(\mathbf{x}, 0) = u_0. \tag{1}$$

Obviously, the solution $u = u(\mathbf{x}, t)$ exists and it is unique and can be determined by means of the method of characteristics provided $\mathbf{v}$ is smooth enough (say, C^1). In this case, for all initial datum $u_0 \in L^2(\mathbb{R}^2)$ there exists a unique solution in the class $C([0, T]; L^2(\mathbb{R}^2))$.

The inverse design problem can be stated as follow: given $\Omega \subset \mathbb{R}^2$, and a target function $u^* = u^*(\mathbf{x})$, determine the initial condition u_0 such that the corresponding solution of Eq. (1) satisfies $u(\mathbf{x}, T) = u_T$ for all $\mathbf{x} \in \Omega$.

This problem can be easily addressed from the point of view of optimal control. To this end, let us introduce the following functional measuring the quadratic error with respect to the target function u_T:

$$J(u_0) = \frac{1}{2} \int_\Omega (u(\cdot, T) - u_T)^2 \, d\mathbf{x}. \tag{2}$$

The inverse design problem then translates in the following optimization one:

$$\widehat{u}_0 = \min_{u_0 \in L^2(\mathbb{R}^N)} J(u_0). \tag{3}$$

This problem (3) is typically solved via a gradient descent (GD) algorithm as follows:

$$\begin{aligned} \widehat{u}_0 &= \lim_{k\to+\infty} u_0^k \\ u_0^{k+1} &= u_0^k - \eta \nabla J(u_0^k). \end{aligned} \tag{4}$$

We then need to compute the gradient ∇J. To this end, let us first rewrite Eq. (1) in non-divergence form, that is

$$\begin{cases} \dfrac{\partial u}{\partial t} + \mathbf{v}\cdot\nabla u = 0, \\ u(\mathbf{x},0) = u_0. \end{cases}$$

Let us now introduce the Lagrangian

$$\mathcal{L}(u,\sigma) := \frac{1}{2}\int_\Omega (u(\cdot,T) - u_T)^2\, d\mathbf{x} + \int_0^T \int_\Omega \sigma \left(-\frac{\partial u}{\partial t} - \mathbf{v}\cdot\nabla u \right) d\mathbf{x}dt$$

and compute the directional derivative $\delta\mathcal{L}(u,\sigma)$ as

$$\delta\mathcal{L}(u,\sigma) = \int_\Omega (u(\cdot,T) - u_T)\delta u(\cdot,T)\, d\mathbf{x} + \int_0^T \int_\Omega \sigma \left(-\frac{\partial \delta u}{\partial t} - \mathbf{v}\cdot\nabla \delta u \right) d\mathbf{x}dt. \tag{5}$$

We now integrate by parts the last term in the above expression, obtaining

$$\begin{aligned} &\int_0^T \int_\Omega \sigma \left(-\frac{\partial \delta u}{\partial t} - \mathbf{v}\cdot\nabla \delta u \right) d\mathbf{x}dt \\ &\quad = -\int_\Omega \sigma(\cdot,T)\delta u(\cdot,t)\, d\mathbf{x} + \int_\Omega \sigma(\cdot,0)\delta u(\cdot,0)\, d\mathbf{x} \\ &\qquad + \int_0^T \int_\Omega \left(\frac{\partial \sigma}{\partial t} + \mathbf{v}\cdot\nabla\sigma \right) \delta u\, d\mathbf{x}dt. \end{aligned}$$

We then obtain from Eq. (5) that

$$\begin{aligned} \delta\mathcal{L}(u,\sigma) = &\int_\Omega \big(u(\cdot,T) - u^* - \sigma(\cdot,T)\big)\delta u(\cdot,T)\, d\mathbf{x} + \int_\Omega \sigma(\cdot,0)\delta u(\cdot,0)\, d\mathbf{x} \\ &+ \int_0^T \int_\Omega \left(\frac{\partial \sigma}{\partial t} + \mathbf{v}\cdot\nabla\sigma \right) \delta u\, d\mathbf{x}dt \end{aligned}$$

or, equivalently,

$$\delta\mathcal{L}(u,\sigma) = \int_\Omega \sigma(\cdot,0)\delta u(\cdot,0)\, d\mathbf{x}$$

with the constraint that σ is a solution of the adjoint (backward) equation

$$\begin{cases} \dfrac{\partial \sigma}{\partial t} + \mathbf{v} \cdot \nabla \sigma = 0, \\ \sigma(\mathbf{x}, T) = u(\mathbf{x}, T) - u_T. \end{cases} \tag{6}$$

This, in particular, tells us that the gradient ∇J is given by

$$\nabla J = \sigma(\cdot, 0)$$

and, consequently, the iterative scheme (4) becomes

$$u_0^{k+1} = u_0^k - \eta \sigma^{\,k}(0)$$

where, in each iteration, we need to solve the following coupled system

$$\begin{cases} \dfrac{\partial u^k}{\partial t} + \nabla \cdot (\mathbf{v} u^k) = 0, \quad u^k(\mathbf{x}, 0) = u_0^k \\ \dfrac{\partial \sigma^{\,k}}{\partial t} + \mathbf{v} \cdot \nabla \sigma^{\,k} = 0, \quad \sigma^{\,k}(\mathbf{x}, T) = u^k(\mathbf{x}, T) - u_T. \end{cases} \tag{7}$$

The GD algorithm is based on iterating a loop, where the transport equation (1) is solved in a forward sense, while the adjoint equation (6), which is of hyperbolic nature as well, is solved in a backward sense.

3. The $MMOC$

Characteristic-based methods provide computationally efficient approximations of the solution of linear transport equations. Douglas and Russel [2] introduced an Eulerian-Lagrangian scheme based on the characteristic curve, called $MMOC$, to develop fast solvers for transport equations. Despite the $MMOC$ does not preserve, as an algebraic identity, a desired conservation law associated with the underlying physical problem, it allows for using large time steps in a simulation without loss of accuracy [4, 5].

Considering that the velocity field is divergence-free ($\nabla \cdot \mathbf{v} = 0$), the Eq. (1) in non-conservative form is

$$\frac{\partial u}{\partial t} + \mathbf{v} \cdot \nabla u = 0. \tag{8}$$

The solution of Eq. (6) is essentially along the characteristic curves of the transport operator $\partial/\partial t + \mathbf{v} \cdot \nabla$, so that it is appropriate to introduce differentiation in this characteristic direction. Let

$$\partial/\partial t + \mathbf{v} \cdot \nabla = \psi \frac{\partial}{\partial \tau}, \quad \psi(u) = \sqrt{1 + \|\mathbf{v}\|^2}, \tag{9}$$

in which the direction τ depends on $\mathbf{x}$.

Let us consider the discretization of Eq. (6) in time. Denote the time step $\Delta t > 0$ and consider the approximation of the solution at times $t^n = n\Delta t$. In the standard $MMOC$, the characteristic derivative is approximated by

$$\psi \frac{\partial u}{\partial \tau} \approx \psi(u(\mathbf{x}, t^n)) \frac{u(\mathbf{x}, t^{n+1}) - u(\overline{\mathbf{x}}, t^n)}{\sqrt{\|\mathbf{x} - \overline{\mathbf{x}}\|^2 + (\Delta t)^2}} = \frac{u(\mathbf{x}, t^{n+1}) - u(\overline{\mathbf{x}}, t^n)}{\Delta t}, \tag{10}$$

where the predecessor position is

$$\overline{\mathbf{x}} = \overline{\mathbf{x}}(\mathbf{x}) = \mathbf{x} - \mathbf{v}(\mathbf{x})\Delta t. \tag{11}$$

Let $u^n(\mathbf{x})$ denote the continuous in space approximation to $u(\mathbf{x}, t^n)$. For the predecessor position, the transported function is defined as

$$\overline{u}^n(\mathbf{x}) = u(\overline{\mathbf{x}}, t^n). \tag{12}$$

As the continuous in space approximation for Eq. (10) is

$$\frac{u^{n+1}(\mathbf{x}) - \overline{u}^n(\mathbf{x})}{\Delta t} = 0, \tag{13}$$

then the $MMOC$ scheme is given by

$$u^{n+1}(\mathbf{x}) = \overline{u}^n(\mathbf{x}). \tag{14}$$

For two-dimensional problems, an approximation to the transported function $\overline{u}^n$ is evaluated as the pointwise bilinear interpolant of $u^n(\mathbf{x})$ at the nearest-four grid points that are neighbors of $\overline{\mathbf{x}}$ [6].

4. Numerical simulations

We performed simulations of the Doswell frontogenesis problem, in which $\mathbf{v} = (-yw,\ xw)$ is the velocity field of a steady circular vortex with angular velocity

$$w = \frac{v_T}{\sqrt{x^2 + y^2}}, \tag{15}$$

where v_T is the tangential velocity given by

$$v_T = \overline{v}\ sech^2(\sqrt{x^2 + y^2})\ tanh(\sqrt{x^2 + y^2}), \tag{16}$$

where $\overline{v}$ is a value for which the maximum value of v_T never exceeds the unity. We set $\overline{v} = 2.59807$ for resulting $v_T = 1.0$, and centered the vortex at the origin in order to define, for the Eq. (1), the following initial condition [7] [8]:

$$u(x, y, 0) = tanh(\frac{y}{\delta}), \tag{17}$$

where δ is a constant representing the smoothness of the front zone. A value of $\delta = 1.0$ generates a smooth solution, and a value of $\delta = 1.0 \times 10^{-6}$ gives a sharp front in the initial condition. The solution is considered smooth if it is differenciable everywhere on its domain. The exact solution for this condition is given by

$$u(x, y, t) = tanh(\frac{y\ cos(wt) - x\ sin(wt)}{\delta}), \tag{18}$$

For our simulations, the time step was restricted by the CFL condition [9], which can be expressed for equal grid-spacing by

$$\Delta t = CFL\frac{\Delta x}{\max v}, \quad CFL \leq 1.0, \tag{19}$$

where $\Delta x\ (= \Delta y)$ is the space step, and v is the component velocity. The Courant number in the simulations was set $CFL = 0.5$.

Let u_i^n denote the numerical approximation to $u(\mathbf{x}_i, t^n)$, at grid points. The accuracy is evaluated through the computation of some error in the simulations. The root mean squared (RMS) error of the numerical schemes is given by

$$e(u) = \sqrt{\frac{1}{N}\sum_{i=1}^{N}(u_i^n - u(\mathbf{x}_i, t^n))^2}, \tag{20}$$

where N is the number of grid points.

The LF and LW schemes were used for comparisons of computational performance. Table 1 describes the numerical schemes for one-dimensional problems. The convergency and accuracy properties of the schemes must be proved in order to gain confidence in the numerical result. Theoretical analysis of convergence and accuracy of the LF and LW schemes for linear advection problems can be found in [10]. Under the CFL condition, the LF scheme is accurate of $O(\Delta t + \Delta x^2)$, and the LW scheme, $O(\Delta t^2 + \Delta x^2)$. In [11], it was shown that the rate of convergence of the $MMOC$ scheme for linear advection problems is optimal with continuous piecewise linear approximating spaces. In this case, the accuracy of the $MMOC$ scheme is of $O(\Delta t + \Delta x^r)$, with $r = \min(s, 1)$, where s is related to the smoothness of the solution.

Table 1: Description of the one-dimensional schemes.

Scheme	*Formulation*
LF	$u_i^{n+1} = \frac{1}{2}\left(u_{i+1}^n + u_{i-1}^n\right) - \frac{1}{2}v_i\frac{\Delta t}{\Delta x}\left(u_{i+1}^n - u_{i-1}^n\right)$
LW	$u_i^{n+1} = u_i^n - \frac{1}{2}v_i\frac{\Delta t}{\Delta x}\left(u_{i+1}^n - u_{i-1}^n\right) + \frac{1}{2}v_i^2\frac{\Delta t^2}{\Delta x^2}\left(u_{i+1}^n - 2u_i^n + u_{i-1}^n\right)$
$MMOC$	$u_i^{n+1} = u(\overline{x}_i, t^n),\ \overline{x}_i = x_i - v_i\Delta t$

For two-dimensional problems, we used dimensional splitting. In this approach a two-dimensional problem is split into two one-dimensional problems, and each one is solved sequentially by using an one-dimensional scheme [9].

4.1. Forward simulations

First, forward simulations were carried out in order to check the order of magnitude of the RMS error, which results are compared with two cases found in the literature. In Case 1 [12], the problem was simulated using a second-order space-centered scheme and a third-order Runge-Kutta time-stepping scheme for the domain $\Omega = [-5, 5]^2$, smoothness of the front zone $\delta = 0.05$, $\overline{v} = 2.58$, and $T = 4.5s$. In Case 2 [13], it was used the Lax-Wendroff scheme on structured rectilinear grid for the domain $\Omega = [-4, 4]^2$, smoothness of the front zone $\delta = 2.0$, $\overline{v} = 2.5974$, and $T = 4.0s$. Table 2 presents the error according to the space step. The results from our LW scheme are in good agreement with both cases. We remark that the definition of RMS error in Case 2 is slightly different from the Eq. (20).

Table 2: Error checking in forward simulations.

Δx	Case 1	LW
0.02	8.4×10^{-2}	7.0×10^{-2}
0.04	1.4×10^{-1}	1.0×10^{-1}
0.08	1.7×10^{-1}	1.4×10^{-1}
Δx	Case 2	LW
0.08	3.4×10^{-4}	1.5×10^{-4}
0.16	1.1×10^{-3}	7.8×10^{-4}
0.32	3.7×10^{-3}	3.5×10^{-3}

Next, forward simulations were carried out for the domain $\Omega = [-5, 5]^2$ considering that the smoothness of the front zone is $\delta = 1.0$, and $\overline{v} = 2.59807$. In this condition, the solutions over the time are moving smooth vortex-type surfaces. The initial condition and exact solution at $T = 4.0s$ can be seen in Fig. 1.

The RMS error in numerical solutions with the domain Ω discretized by 160×160 grid, at different times can be seen in Table 3. The error increases as the simulation time is increased, for all schemes. The LF scheme provides the largest

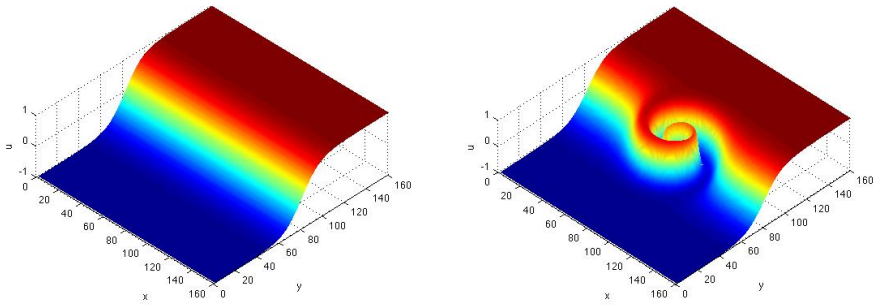

Figure 1: The initial condition (left) and exact solution at $T = 4.0s$ (right) with $\delta = 1.0$.

error at all times, since it introduces high numerical diffusion as a first-order scheme. The LW scheme is more accurate than the others, in spite of producing spurious oscillations at the vortex zone. The $MMOC$ scheme introduces some numerical errors due to the bilinear interpolation. It is known that interpolation may cause numerical dispersion and attenuation in characteristic-based methods [14].

Table 3: Error over time in the forward simulation.

	LF	LW	$MMOC$
$T\ (s)$		$e(u_T)$	
4.0	1.40×10^{-1}	1.64×10^{-2}	6.14×10^{-2}
6.0	1.89×10^{-1}	3.70×10^{-2}	1.00×10^{-1}
8.0	2.24×10^{-1}	6.65×10^{-2}	1.26×10^{-1}

Another performance measure of numerical schemes is the order of accuracy. The higher the order of accuracy, the faster the numerical error is reduced as Δx decreases. The order of accuracy can be computed by [15]

$$p(u) = \frac{ln\ e(u)|_{2\Delta x} - ln\ e(u)|_{\Delta x}}{ln\ 2}. \tag{21}$$

A convergence study of the error in space discretization was conducted by solving the Doswell frontogenesis problem in forward sense. The error and order of accuracy in numerical solutions at $T = 4.0s$ are showed in Table 4.

Table 4: Convergence study in the forward simulation.

LF		
Δx	$e(u_T)$	$p(u_T)$
0.5	2.78×10^{-1}	–
0.25	2.24×10^{-1}	0.31
0.125	1.79×10^{-1}	0.32
0.0625	1.40×10^{-1}	0.35
0.03125	1.07×10^{-1}	0.39
0.015625	7.60×10^{-2}	0.49
LW		
Δx	$e(u_T)$	$p(u_T)$
0.5	1.56×10^{-1}	–
0.25	9.69×10^{-2}	0.69
0.125	4.17×10^{-2}	1.22
0.0625	1.64×10^{-2}	1.35
0.03125	6.74×10^{-3}	1.28
0.015625	2.98×10^{-3}	1.17
$MMOC$		
Δx	$e(u_T)$	$p(u_T)$
0.5	1.57×10^{-1}	–
0.25	1.20×10^{-1}	0.39
0.125	8.97×10^{-2}	0.42
0.0625	6.14×10^{-2}	0.55
0.03125	3.83×10^{-2}	0.68
0.015625	2.21×10^{-2}	0.79

The decrease of the error as a function of the grid refinement is observed for all schemes, indicating that the numerical solutions tend to converge to the exact solution. The LW scheme provides the highest order of accuracy, followed by the $MMOC$ scheme. The LW scheme achieves the maximum order of accuracy

with $\Delta x = 0.0625$ (160×160 grid). The LW scheme exhibits order of accuracy slightly greater than 1 because of the spurious oscillations within the numerical solution. In computational applications where the order of accuracy is measured 'experimentally', the estimation of the order of accuracy might be inaccurate when solving problems in which the solution is not sufficiently smooth.

4.2. Inverse design simulations

The GD algorithm for addressing the problem of inverse design is divided into two steps: forward and backward resolutions. In the first, the primitive equation is numerically solved forward in time; in the next, the adjoint equation is solved backward in time. It is compulsory to solve the primitive equation by means of high-order schemes to guarantee sufficient accuracy in simulations. However, high-order schemes provide spurious oscillations when solving the adjoint equation. These spurious oscillations slow down the convergence of the algorithm. In [1] it was showed the convenience of using a first-order scheme for solving the adjoint equation, both in terms of accuracy and efficiency.

Thus, our inverse design simulations was performed by using the LW scheme in the resolution in forward sense, and the LW and $MMOC$ schemes for the adjoint problem, denoting the two numerical strategies by $LW - LW$ and $LW - MMOC$, respectively. The use of the LF scheme was discarded since it provides high numerical diffusion. In tests with $LW - LF$, large errors was observed for both inicial condition and target function.

The GD algorithm was run assuming $\epsilon = 0.5$ as gradient step size, the exact solution at $T = 4.0s$ as target function, and $u_0 = 0.0$ as initial guess. Moreover, we choosed the stopping criterion to be the L_2 relative error between current and previous solutions in the GD algorithm with tolerance $TOL = 10^{-4}$.

Considering the domain $\Omega = [-5, 5]^2$ discretized by 160×160 grid, the exact solution at $T = 4.0s$, and the smoothness of the front zone $\delta = 1.0$, the initial condition and target function for the numerical strategies can be observed in Fig. 2. There is a trace of spurious oscillations near the vortex zone in the initial condition with the $LW - LW$; this effect is reduced with the $LW - MMOC$.

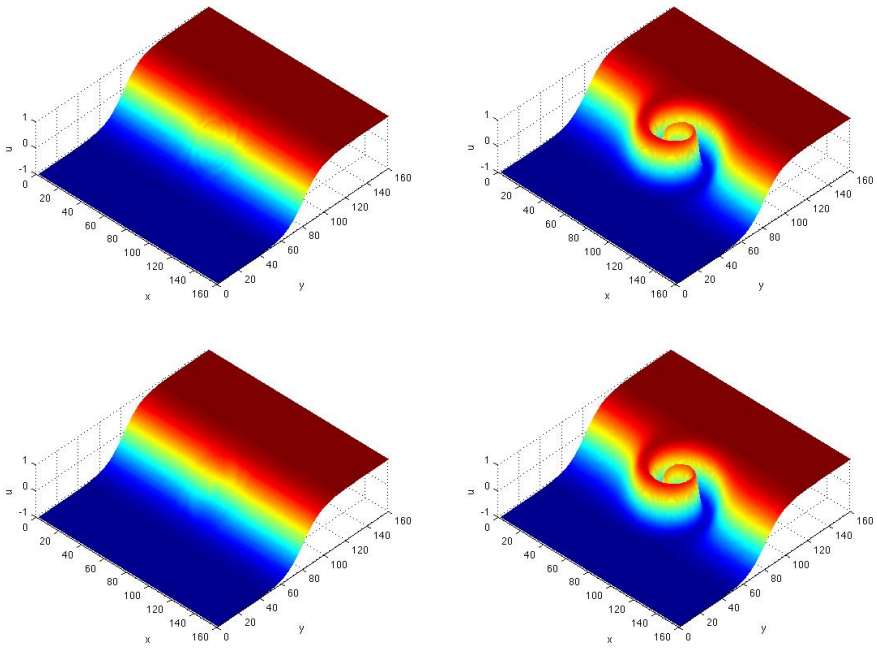

Figure 2: The initial condition (left) and target solution at $T = 4.0s$ (right) with $\delta = 1.0$, by $LW - LW$ (top) and $LW - MMOC$ (bottom).

The computational performance of the numerical strategies is shown in Table 5. For the sake of clarity in the comparison, the best results are highlighted in bold font. Despite the $LW - MMOC$ provides the most accurate simulation for the initial condition, the $LW - LW$ is the most computationally efficient. As expected, the $LW-LW$ have the most accurate simulation for the target function, since second-order schemes are more convenient to the forward resolution. The good performance with the $LW - LW$ in smooth solutions is already expected once the LW scheme presented the higher order of accuracy.

Table 5: Inverse design simulation with $\delta = 1.0$.

Strategy	*Iteration*	*CPU* time (s)	$e(u_0)$	$e(u_T)$
$LW - LW$	**40**	**151.1**	1.71×10^{-2}	$\mathbf{1.37 \times 10^{-3}}$
$LW - MMOC$	66	254.2	$\mathbf{1.33 \times 10^{-2}}$	8.46×10^{-3}

In order to check the effect of some parameters on the computational performance of the numerical strategies, more severe situations were tested for the inverse design simulation by changing the grid-spacing, solution time and smoothness of the front zone. The Table 6 shows the alternative situations used for this study.

Table 6: The alternative situations for the simulation study.

Situation	*Grid*	*Time* (s)	*Smoothness*
Standard	160×160	4.0	1.0
Coarser grid	80×80	4.0	1.0
Longer time	160×160	8.0	1.0
Sharper front	160×160	4.0	1.0×10^{-6}

Firstly, an alternative simulation is performed with a coarser grid. In Table 7, it is showed the performance of the numerical strategies considering the domain discretized by 80×80 grid. In this coarser grid, the $LW - MMOC$ provides a better computational performance than the $LW - LW$. Multi-scale features will be eventually be developed in the solution of the Doswell frontogenesis problem, which is beyond the resolution of the grid being considered [16]. Fine scale features are developed near the origin, where the vortex flow is strongest. The coarse resolution of the fine scale features by second-order schemes provides spurious oscillations within the solution [12]. This justify the worst result of the $LW - LW$ for the coarser grid.

Table 7: The alternative simulation with 80×80 grid.

Strategy	*Iteration*	*CPU* time (s)	$e(u_0)$	$e(u_T)$
$LW - LW$	278	133	6.18×10^{-2}	$\mathbf{6.21 \times 10^{-3}}$
$LW - MMOC$	**157**	**76**	$\mathbf{2.91 \times 10^{-2}}$	2.21×10^{-2}

Secondly, an alternative simulation is performed by assuming the exact solution at $T = 8.0s$ as target function. As time evolves, the multi-scale features in the solution are exacerbated. Thus, a challenging situation is posed to the

$LW - LW$, once it introduces high frequencies and spurious oscillations near the vortex zone, where there are more fine scale features. The results of performance of the numerical strategies are shown in Table 8. The $LW - MMOC$ provides the best computational performance.

Table 8: The alternative simulation with target function at $T = 8.0s$.

Strategy	*Iteration*	*CPU* time (s)	$e(u_0)$	$e(u_T)$
$LW - LW$	455	3445.5	1.07×10^{-1}	$\mathbf{1.18 \times 10^{-2}}$
$LW - MMOC$	**362**	**2789.5**	$\mathbf{4.42 \times 10^{-2}}$	7.22×10^{-2}

Lastly, the inverse design simulation of the Doswell frontogenesis problem is performed with the smoothness of the front zone $\delta = 1.0 \times 10^{-6}$. For this situation, sharp fronts are expected to appear over the time. It is well known that solutions with sharp fronts where high frequencies and spurious oscillations play an important role require a filtering or smoothing operator to eliminate the undesirable oscillations that appear when trying to solve the adjoint problem in backward sense. First-order schemes as the $MMOC$ for the adjoint resolution play the same role of a filtering or smoothing operator to eliminate the undesirable oscillations [17, 18, 19]. The initial condition and exact solution at $T = 4.0s$ with $\delta = 1.0 \times 10^{-6}$ are shown in Fig. 3.

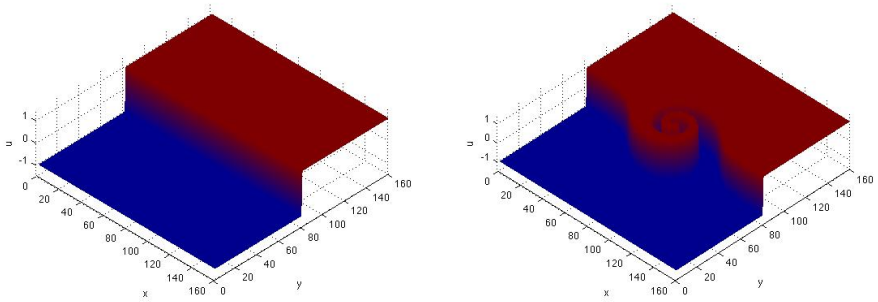

Figure 3: The initial condition (left) and solution at $T = 4.0s$ (right) with $\delta = 1.0 \times 10^{-6}$.

As the $LW - LW$ introduces high frequencies and spurious oscillations in sharp front solutions, the convergence in the GD algorithm is slower achieved.

Thus, a maximum number of iteration of 300 was implemented for this simulation. The result of performance of the numerical strategies are shown in Table 9. Once more, the $LW - MMOC$ provides the best computational performance.

Table 9: The alternative simulation with $\delta = 1.0 \times 10^{-6}$.

Strategy	*Iteration*	*CPU* time (s)	$e(u_0)$	$e(u_T)$
$LW - LW$	300	1132.5	3.03×10^{-1}	$\mathbf{6.67 \times 10^{-2}}$
$LW - MMOC$	**251**	**966.1**	$\mathbf{1.21 \times 10^{-1}}$	1.09×10^{-1}

The initial condition and target function at $T = 4.0s$ from the numerical strategies with $\delta = 1.0 \times 10^{-6}$ are illustrated in Fig. 4. There are high spurious oscillations near the vortex zone in the solutions by the $LW - LW$, while effects of dissipation are noted in the vortex zone with the $LW - MMOC$. In both initial condition and target function the shape of the solution is better defined with the $LW - MMOC$.

5. Conclusions

The problem of inverse design of linear transport equations can be addressed by using several strategies combining the schemes LW and $MMOC$. The performance of the numerical strategies depends on the test case under simulation in which fronts and discontinuities can be propagated over the space and time.

In the inverse design simulations of the Doswell frontogenesis problem, we considered as a reference for comparisons the following situation: the domain discretized by 160×160 grid, the exact solution at $T = 4.0s$ as target function, and the smoothness of the front zone $\delta = 1.0$. Under this situation, the $LW - LW$ showed to be more computationally efficient than the $LW - MMOC$, in spite of the last one be more accurate with respect to the initial condition.

However, we have identified alternative situations in which the $LW - MMOC$ provides shorter CPU time and higher accuracy than the $LW - LW$, in the inverse design simulation of the Doswell frontogenesis problem. These results were obtained when considering coarser grid, target function at longer time, and

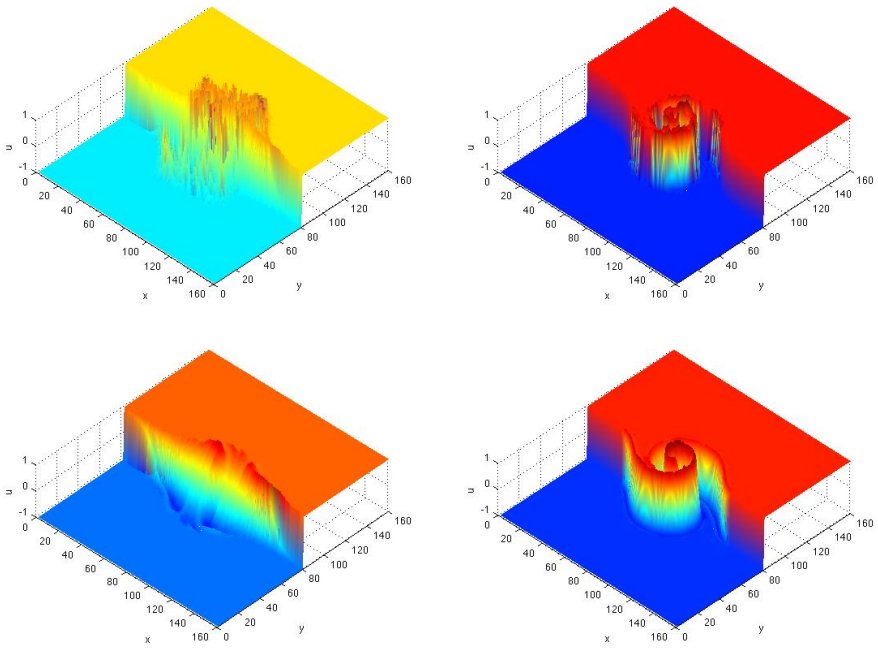

Figure 4: The initial condition (left) and solution at $T = 4.0s$ (right) with $\delta = 1.0 \times 10^{-6}$, by $LW - LW$ (top) and $LW - MMOC$ (bottom).

sharper front solution. In these alternative situations, the second-order scheme introduced high frequencies and spurious oscillations in the solutions. Thus, the $LW - MMOC$ have presented the most efficient and accurate computation in more severe situations used for the inverse design simulation.

The $MMOC$ is a promising characteristic-based scheme for addressing the problem of inverse design of linear transport equations, under some simulation conditions. The computational performance with this numerical scheme are to be checked for nonlinear transport equations.

Acknowledgements

Part of this research was carried out at the Fundacion Deusto and University of Deusto with the financial support of the DyCon Project (ERC Advanced Grant 2015 H2020-694126) and Brazilian agency FAPERJ (Grant E-26/203.107/2019).

References

References

[1] M. Morales-Hernandez, E. Zuazua, Adjoint computational methods for 2d inverse design of linear transport equations on unstructured grids, Computational and Applied Mathematics (2019) 167–192.

[2] J. Douglas, T. F. Russell, Numerical methods for convection dominated diffusion problems based on combining the method of characteristics with finite element or finite difference procedures, SIAM J. Numer. Anal. (1982) 871–885.

[3] C. Zhang, X. Li, C. Yang, A modified method of characteristic and its application in forward and inversion simulations of underwater explosion, AIP Advances (2016) 1–14.

[4] J. Douglas, C. S. Huang, F. Pereira, The modified method of characteristics with adjusted advection for an immiscible displacement problem, Lecture Notes in Pure and Applied Mathematics (1999) 53–74.

[5] R. Ewing, H. Wang, A summary of numerical methods for time-dependent advection dominated partial differential equations, Journal of Computational and Applied Mathematics (2001) 423–445.

[6] J. Douglas, F. Furtado, F. Pereira, On the numerical simulation of waterflooding of heterogeneous petroleum reservoirs, Computational Geosciences (1997) 155–190.

[7] C. A. Doswell, A kinematic analysis of frontogenesis associated with a nondivergent vortex, Journal of the Atmospheric Sciences (1983) 1442–1248.

[8] V. S. K. Nair, High-order numerical schemes for compressible flows, Ph.D. thesis, Delft University of Technology, Illinois, VS, US (2016).

[9] R. J. Leveque, Finite difference methods for ordinary and partial differential equations, SIAM, Philadelphia, US, 2007.

[10] J. C. Strikwerda, Finite difference schemes and partial differential equations, SIAM, Philadelphia, US, 2004.

[11] C. N. Dawson, T. F. Dupont, M. F. Wheeler, The rate of convergence of the modified method of characteristics for linear advection equations in one dimension, Technical Report 88-3 (1988) 1 – 11.

[12] K.-A. Tan, R. P. Morison, L. M. Leslie, A comparison of high-order explicit and non-oscillatory finite difference advection schemes for climate and weather models, Meteorology and Atmospheric Physics (2005) 251–267.

[13] N. Ahmad, Z. Boybeyi, R. Lohner, A. Sarma, A godunov-type finite-volume scheme for flows on the meso- and micro-scales, American Institute of Aeronautics and Astronautics (2005) 1 – 20.

[14] J. Twyman, Transient flow analysis using the method of characteristics moc with five-point interpolation scheme, Obras y Proyectos (2018) 62–70.

[15] N. Ahmad, F. Proctor, Advection of microphysical scalar in terminal area simulation system (tass), in: Annals of 49th AIAA Aerospace Sciences Meeting, The Organization, Orlando, USA, 2011.

[16] V. Titarev, E. Toro, Finite volume weno schemes for three dimensional conservation laws, Journal Computational Physics (2004) 238 – 260.

[17] G. Dogan, P. Morin, R. H. Nochetto, M. Verani, Discrete gradient flows for shape optimization and applications, Computational Methods in Applied Mechanical Engineering (2007) 3898 – 3914.

[18] S. Everdoza, E. Zuazua, On the numerical approximation of exact controls for waves, Springer Briefs in Mathematics, ISBN 978-1-4614-5808-1, 2013.

[19] E. Zuazua, Propagation, observation, and control of waves approximately by finite difference methods, SIAM Rev 47(2) (2005) 197 – 243.